Physics of Plasmas

RESEARCH ARTICLE | JULY 10 2024

Electromagnetic ion cyclotron emission from ion-scale magnetic holes

Muhammad Shahid ; M. Fraz Bashir ; Anton V. Artemyev ; Xiao-Jia Zhang ; Vassilis Angelopoulos ; G. Murtaza

Phys. Plasmas 31, 072103 (2024)
https://doi.org/10.1063/5.0205942

Electromagnetic ion cyclotron emission from ion-scale magnetic holes

Cite as: Phys. Plasmas **31**, 072103 (2024); doi: 10.1063/5.0205942
Submitted: 28 February 2024 · Accepted: 19 June 2024 ·
Published Online: 10 July 2024

Muhammad Shahid,[1,2] M. Fraz Bashir,[2,a)] Anton V. Artemyev,[2,3] Xiao-Jia Zhang,[2,4] Vassilis Angelopoulos,[2] and G. Murtaza[1]

AFFILIATIONS

[1]Salam Chair in Physics, Government College University Lahore, Lahore 54000, Pakistan
[2]Department of Earth, Planetary, and Space Sciences, University of California, Los Angeles, California 90095, USA
[3]Space Research Institute, Russian Academy of Sciences, Moscow 117997, Russia
[4]Department of Physics, The University of Texas at Dallas, Richardson, Texas 75080, USA

[a)]**Author to whom correspondence should be addressed:** frazbashir@epss.ucla.edu

ABSTRACT

Ion-scale magnetic holes are nonlinear plasma structures commonly observed in the solar wind and Earth's magnetosphere. These holes are characterized by the magnetic field depletion filled by hot, transversely anisotropic ions and electrons and are likely formed during the nonlinear stage of ion mirror instability. Due to the plasma thermal anisotropy within magnetic holes, they serve as a host of electromagnetic ion cyclotron waves, whistler-mode waves, and electron cyclotron harmonic waves. This makes magnetic holes an important element of the Earth's inner magnetosphere, where electromagnetic waves generated within may strongly contribute to energetic ion and electron scattering. Such scattering, however, will modify the hot-ion distribution that is trapped within magnetic holes and responsible for the magnetic field stress balance. Therefore, hot ion scattering within magnetic holes likely determines the hole lifetime. In this study, we investigate how ion scattering by electromagnetic waves affects the stress balance and lifetime of magnetic holes. For illustration, we used typical characteristics of magnetic holes, ion populations, and ion cyclotron waves observed in the Earth's magnetosphere. We have demonstrated that ion distribution isotropization via scattering by waves does not change significantly magnetic hole magnitude, but ion losses due to scattering into the atmosphere may limit the hole life-times to 10–30 min in the Earth's inner magnetosphere.

I. INTRODUCTION

The ion-scale magnetic holes, localized depletions of the magnetic field magnitude, represent one of the quite stable and commonly observed nonlinear plasma structures in the pristine[55,61] and shocked[25,27,58] solar wind, planetary,[12–14,16,17,46,54,66,68] and cometary[19,43,44,51] magnetospheres. Formation of such structures is typically attributed to the nonlinear stage of the ion mirror mode,[8,24,31,40] although smaller (sub-ion) scale magnetic holes may be generated by plasma turbulence[21,41] and various types of acoustic instabilities.[26,32,45]

One important property of magnetic holes is their stability: such holes may travel for large distances in the solar wind.[42] This stability allows magnetic holes generated around the Earth's magnetosphere boundary, magnetopause, to propagate into the inner magnetosphere and transport hot trapped ion and electron populations.[30,64] The stress balance in magnetic holes and their formation mechanism assume that the trapped ion and electron populations are transversely anisotropic and hotter than the plasma background.[37,60] Thus, the transport of these populations into the inner magnetosphere provides an additional energy source for the generation of electromagnetic waves that play an important role in the dynamics of energetic particles.[7,52,67] In fact, spacecraft observations of magnetic holes in the Earth's inner magnetosphere are usually associated with localized bursts of electromagnetic whistler-mode waves,[12,64] electron cyclotron harmonics,[13] and electromagnetic ion cyclotron (EMIC) waves.[30,59,65] The latter wave mode is generated by hot, transversely anisotropic ions[22] trapped within magnetic holes.[5,60]

EMIC waves are quite effective in resonantly scattering hot ions,[9,10,15] and their generation within magnetic holes is expected to result in isotropization of the ion population and precipitation into the atmosphere. Such isotropization and ion losses due to precipitation will alter the hot trapped ion population that is responsible for the pressure balance in magnetic holes. Thus, EMIC waves may influence

the magnetic hole structure by scattering these hot trapped ions. See the schematic diagram in Fig. 1 Such a feedback mechanism will modify the magnetic holes and finally, when a sufficiently large ion population is lost, will destroy the holes. This natural limitation of magnetic hole lifetime in the Earth's inner magnetosphere is the focus of our study.

To illustrate the typical characteristics of the system consisting of magnetic holes, hot transversely anisotropic trapped ions, and EMIC waves, we provide an illustrative Fig. 2 showing the example of THEMIS[2] observations in the inner Earth's magnetosphere. Panel (a) shows several bursts (maxima) of electromagnetic wave emission within the helium and proton cyclotron frequency ranges; the spectrum analysis shows that these are left-hand circularly polarized and field-aligned EMIC waves.[53] The peaks of EMIC wave amplitude [panel (b)] are within local depletion of the background magnetic field shown in panel (c) as negative compressional fluctuations $\delta B_{\parallel} < 0$ of a few nanotesla magnitude; these are magnetic holes. Hot transversely anisotropic ions fill these magnetic field minima: panels (d) and (e) show peaks of ion flux anisotropy (better seen for the >3 keV range) and peaks of ion temperature anisotropy; these peaks coincide with peaks of the EMIC amplitude. The stress balance within magnetic holes is controlled by the hot-ion component: panel (f) shows the variations of magnetic and hot-ion thermal pressures. The EMIC wave generation within magnetic holes is supported by enhanced ion fluxes [see panel (g) for peaks of ion beta] and ion anisotropy. Thus, Fig. 2 shows a typical example of a magnetic hole with trapped hot ions unstable to EMIC wave generation. In this study, we plan to provide estimates of how such EMIC waves interacting resonantly with hot ions may reduce their contribution to the stress balance within magnetic holes, which will eventually determine the hole lifetime.

In this study, we analyze the event shown in Fig. 2 to reveal the potential EMIC wave effect on scattering and losses of the hot ion population trapped within the magnetic hole. In Sec. II, we use the linear analysis of the observed ion distribution function to confirm the generation mechanism of observed EMIC waves. In Sec. III, we estimate the effect of ion isotropization due to scattering by EMIC waves. In Sec. IV we estimate the effect of ion losses from the magnetic hole due to scattering by EMIC waves. Then, in Sec. V we summarize the results obtained and discuss the role of the EMIC wave in the stability of the magnetic hole.

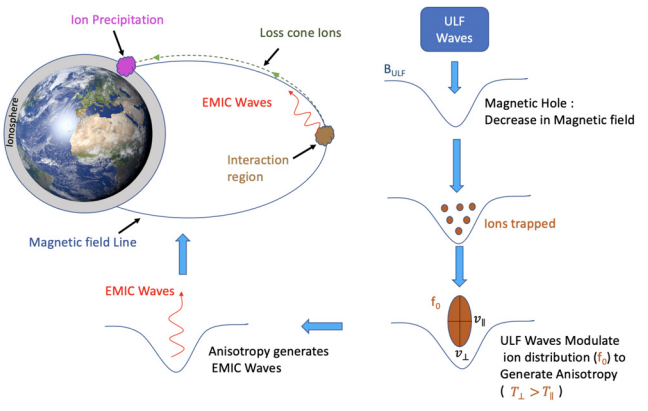

FIG. 1. Schematic diagram represents the EMIC waves emission mechanism from the magnetic hole and resulted ion precipitation.

II. ELECTROMAGNETIC ION CYCLOTRON WAVES

To confirm that the transversely anisotropic ion population trapped within magnetic holes is responsible for the generation of observed EMIC waves, we performed a linear stability analysis of this population.[18,39,48] We fit the ion energy and pitch-angle distribution by the combination of three anisotropic Maxwell functions: cold population with the temperature ~12 eV, warm population with the temperature ~300 eV, and hot population with the temperature ~3.6 keV. The fitting shows that the warm population is field-aligned anisotropic[62] and likely represents local background plasma provided by ion outflow from the Earth's ionosphere. The hot population is transversely anisotropic[11,63] and should be the main free energy source for the generation of EMIC waves. The cold population does not resonate with EMIC waves and contributes a lot to the total plasma density.

We use analytical fitting of the observed ion distribution function from Fig. 3 to evaluate EMIC wave growth rate and dispersion relation using Eq. (1) from Ref. 6. Figure 4(a) shows that the observed EMIC wave dispersion is largely affected by the hot plasma contribution and differs well from the cold plasma dispersion from Ref. 49. The difference of wave numbers, k, for normalized wave frequency $\omega/\Omega_{cp} \sim 0.4$ is about factor ×2, i.e., in hot plasma, EMIC waves have much smaller k and will resonate with smaller energy ions [the resonant energy $\propto (\omega - \Omega_{cp})^2/k^2$, where Ω_{cp} is the proton cyclotron frequency]. This hot plasma effect can be important for consideration of the EMIC wave contribution to the scattering of ions trapped within a magnetic hole. Figure 4(b) compares linear wave growth rate, γ/Ω_{cp} (in blue), and the observed wave intensity spectrum. The linear theory reproduces well the observed frequency range of EMIC waves, which confirms that these waves are indeed generated by ion population trapped within a magnetic hole.

The most unstable frequency rate where the growth rate reaches the maximum value is $\omega/\Omega_{cp} \in [0.3, 0.5]$. Spacecraft observations show that within this frequency range, EMIC waves also have the maximum wave power. Therefore, this comparison shows a good agreement between linear theory results and spacecraft observations.

III. ANALYSIS OF ION SCATTERING EFFECT

Generation of EMIC waves and their following scattering of hot ions should result in ion anisotropy relaxation.[23,24,40] In this section, we estimate the maximum possible effect of such relaxation. The pressure balance across the magnetic hole takes the form of a perturbation equation $B_0\delta B_{\parallel} + 4\pi T_{\perp} n = 0$ connecting the magnetic field depletion magnitude $\delta B_{\parallel}$ and the enhancement of the ion thermal pressure $T_{\perp} n$. The same balance equation after full relaxation of the ion distribution will take a form $B_0\delta B_{\parallel}^{new} + 4\pi T_{\perp}^{new} n = 0$, where $T_{\perp}^{new}$ is the ion perpendicular temperature after scattering by EMIC waves. To determine $T_{\perp}^{new}$, we consider the threshold of EMIC wave generation:

$$\frac{T_{\perp}^{new}}{T_{\parallel}^{new}} = 1 + \frac{S}{(\beta_{\parallel}^{new})^A}, \tag{1}$$

where constants S and A are given by numerical simulation of wave saturation.[23] This equation provides the condition for the final ion anisotropy after ion distribution relaxation to the state when EMIC wave generation will be sufficiently weak (the growth rate will be almost

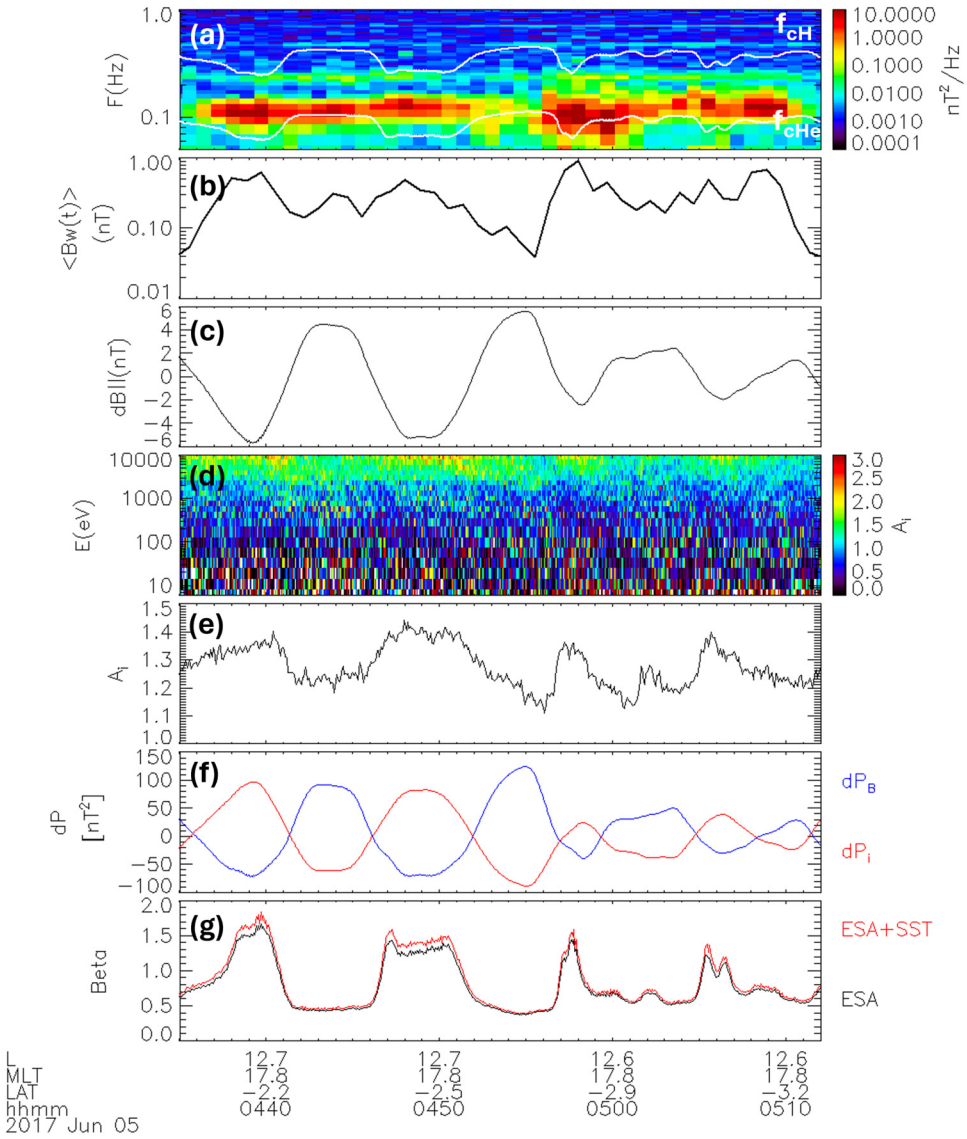

FIG. 2. An example event with EMIC wave emissions from the magnetic holes observed in the Earth's inner magnetosphere by THEMIS-E spacecraft: (a) EMIC wave power spectrum with proton cyclotron and helium cyclotron frequencies shown by white curves, (b) EMIC wave amplitude derived from power spectrum integration, (c) compressional component of the background magnetic field perturbations, (d) energy distribution of ion thermal anisotropy (ratio of perpendicular and parallel ion fluxes) (e) ion temperature anisotropy (ratio of perpendicular and parallel ion pressure components) (f) pressure balance between magnetic field pressure perturbations (shown in blue) and plasma pressure perturbations (shown in red) and (g) ion β (ratio of perpendicular ion pressure and magnetic field pressure). To plot these data, we use measurements of THEMIS fluxgate magnetometer with Fast Survey datatype (1/4s sampling),[4] spin averaged (3s) measurements of ion <25 keV spectra and moments by the Electrostatic Analyzer (ESA)[35] and from 25 keV to 6 MeV by Solid State Telescope (SST). THEMIS data are processed with the SPEDAS software.[3] In this event, THEMIS-E was near the dusk-flank magnetopause, with $X_{GSE} \approx 1.4R_E$, $Y_{GSE} \approx 12.8R_E$, $Z_{GSE} \approx -2.6R_E$; $R_E \approx 6380$ km.

zero). If we take into account that such relaxation is mostly provided by the pitch-angle ion scattering within strong energy redistribution,[24,40] we may add the energy conservation law $2T_\perp^{new} + T_\parallel^{new} = 2T_\perp + T_\parallel$. The combination of these equations and observations of initial $\delta B_\parallel$ and ion anisotropy provides the final $\delta B_\parallel^{new}$. Figure 5 shows the distribution of observations in $(\beta, \delta B_\parallel^{new}/\delta B_\parallel)$ with color coding the initial ion anisotropy. The ion scattering and isotropization can decrease the $nT_\perp$ pressure (and $\delta B_\parallel \propto nT_\perp$) by $\sim$5% for strongly anisotropic and high β case. Such variation of magnetic hole magnitude is not essential, and thus isotropization due to pitch-angle scattering cannot affect the hole lifetime. However, this scattering also provides ion losses, because magnetic holes within the inner magnetosphere are connected along magnetic field lines with the dense ionosphere. Therefore, if EMIC waves are sufficiently effective in scattering small pitch-angle ions, this scattering can drive ion precipitations (see discussion in Refs. 29, 33, and 36). We examine this effect in Sec. IV.

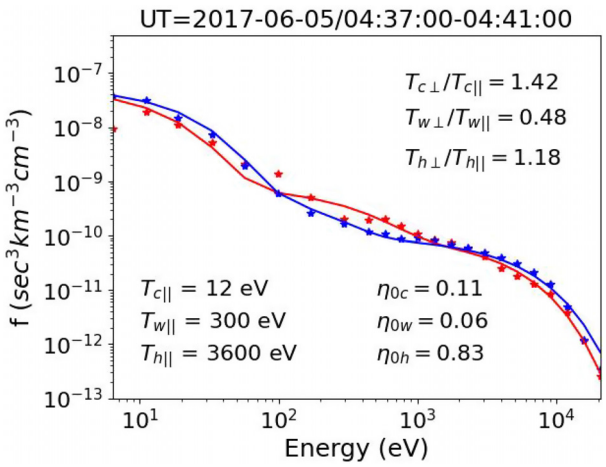

FIG. 3. Observed ion distribution functions (stars) for parallel (blue) and perpendicular (red) pitch-angle ranges during the event in Fig. 2. Curves show fitting of this distribution by a combination of three anisotropic Maxwell functions. Parameters of fitting (parallel temperature, $T_{||}$ anisotropy, $T_\perp/T_{||}$ and relative concentration, η) are indicated in the figure.

IV. ION LOSS

EMIC waves generated by hot ion population within magnetic holes should provide effective pitch-angle scattering of ions. To quantify this scattering, we evaluate the pitch-angle diffusion rate:[6,50]

$$D_{\alpha\alpha} = \frac{\pi}{2}\frac{1}{\nu}\frac{\Omega_{cp}^2}{|\Omega_{ce}|}\frac{R}{(E+1)^2}\frac{\left(1-\frac{x\cos\alpha}{y\beta}\right)^2 e^{-\left(\frac{x-x_m}{\delta x}\right)^2}}{\delta x|F(x,y)|^{-1}\beta\cos\alpha - 1|}, \quad (2)$$

where $\nu = \sqrt{\pi}erf(\sigma)$ with $\sigma = 4/3$ is obtained from observed wave spectrum, $x = \omega/\Omega_{cp}$ is the normalized wave frequency, $y = kc/\Omega_{cp}$ is the normalized wave number, E is the dimensionless particle kinetic energy given by $E = E_k/(m_i c^2)$, $\beta = [E(E+2)]^{1/2}/(E+1)$, $R = B_w^2/B_0^2$ is the ratio of the energy density of the wave magnetic field to that

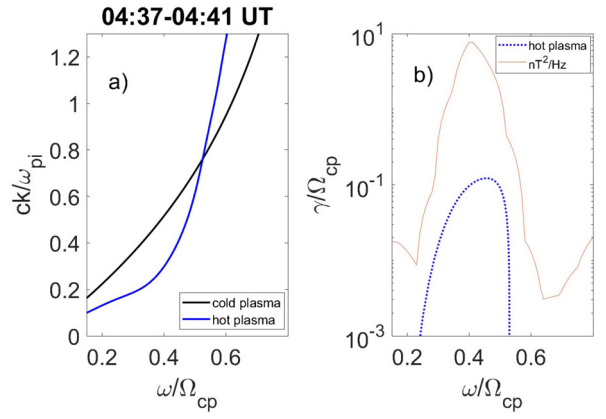

FIG. 4. (a) Normalized wave number ck/ω_{pi} as a function of normalized frequency ω/Ω_{cp} for the cold plasma (black) and observed ion distribution (blue); here ω_{pi} is the ion plasma frequency. (b) Positive growth rate γ/Ω_{cp} as a function of wave frequency and the spectrum of observed EMIC wave intensity in nT^2/Hz.

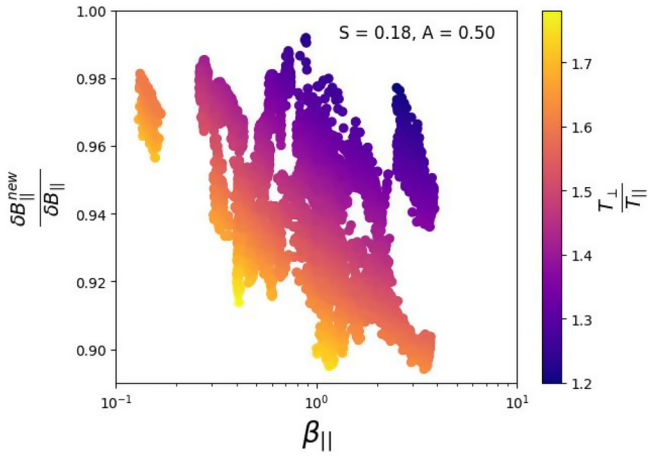

FIG. 5. Initial ion anisotropy ($T_\perp/T_{||}$) in the space of ion beta ($\beta_{||}$) and the ratio ($\delta B_{||}^{new}/\delta B_{||}$) of magnetic hole amplitude ($\delta B_{||}^{new}$) and the initial amplitude $\delta B_{||}$.

of the background field, i.e., the relative wave power; $x_m = w_m/\Omega_{cp}$ and $\delta x = \delta\omega/\Omega_{cp}$ are the normalized maximum and bandwidth frequency respectively, obtained from the characteristics of wave spectrum, and $F(x,y)^{-1} = dy/dx$ is the wave group speed determined from the plasma dispersion of EMIC waves. We used observed spectrum characteristics to set x_m (mean frequency), δx (spectrum dispersion), and R parameters. Figure 6(a) shows $D_{\alpha\alpha}$ [Eq. (2)] for several typical ion energies. There is a fairly strong scattering, with $D_{\alpha\alpha} \sim 10^{-3}$ s^{-1}, of low pitch angle ions for the [2, 10] keV range. This is the ion population that is largely responsible for the pressure balance within a magnetic hole, whereas scattering of these ions may result in their precipitation and loss into Earth's atmosphere. The typical loss-cone size, the pitch-angle range of ions precipitating into the atmosphere, for radial distances of magnetic hole observations is $\Delta\alpha_{LC} \sim 1^\circ$, whereas the bounce period of field-aligned ions of ~5 keV energies is $\tau_b \approx 4$ min. Therefore, $D_{\alpha\alpha} \sim 10^{-3}$ s^{-1} well exceeds the strong diffusion limit, $D_{SD} \approx (\Delta\alpha_{LC})^2/\tau_b \sim 10^{-6}$ s^{-1}, and EMIC waves will always keep the loss-cone full.[28]

This estimate of ion losses should be corrected by the fact that bouncing ions will resonate with EMIC waves only on such a range of off-equatorial distances, i.e., the bounce averaged diffusion rate should be smaller than the local (equatorial) rate. To estimate this bounce averaged $\langle D_{\alpha\alpha}\rangle$, we adopted a dipole field to approximate the Earth's magnetic field topology, $B_0 = B_{eq}\sqrt{1+3\sin^2\lambda}/\cos^6\lambda$, where λ is the magnetic latitude. The local ion pitch-angle can then be recalculated to the equatorial pitch-angle as $\sin\alpha = \sin\alpha_{eq}(1+3\sin^2\lambda)^{1/4}/\cos^3\lambda$. The bounce average diffusion rate is given as follows:[20,34]

$$\langle D_{\alpha_{eq}}\rangle = \frac{1}{T(\alpha_{eq})}\int_0^{\lambda_m} D_{\alpha\alpha}\frac{\cos\alpha}{\cos^2\alpha_{eq}}\cos^7\lambda d\lambda, \quad (3)$$

where $T(\alpha_{eq}) = 1.30 - 0.56\sin\alpha_{eq}$ is the dimensionless ion bounce period.[38] Figure 6(b) shows $\langle D_{\alpha\alpha}\rangle$ profiles [Eq. (3)]: the bounce averaging reduces the diffusion rate magnitude to $\sim 5\times10^{-4}$ s^{-1} and cover the entire range of small pitch-angles. Using $\langle D_{\alpha\alpha}\rangle$, we may evaluate ion lifetime:[1]

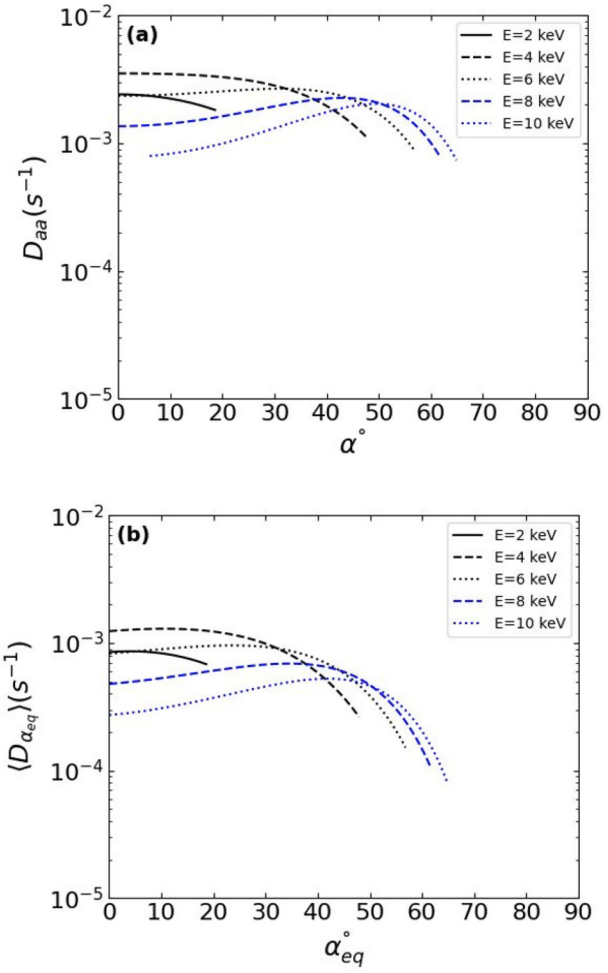

FIG. 6. (a) Local pitch-angle diffusion rates $D_{\alpha\alpha}$ vs α for EMIC waves interacting with protons of different kinetic energies. (b) Bounce-averaged pitch angle diffusion coefficient $\langle D_{\alpha_{eq}}\rangle$ as a function of equatorial pitch angle α_{eq} due to interactions between ions with H^+ band for different energies i.e., E = (2, 4, 6, 8, 10) keV.

$$\tau^* = \int_{\Delta\alpha_{LC}}^{\alpha_{\max}} \frac{d\alpha_{eq}}{2\langle D_{\alpha\alpha}\rangle \tan\alpha_{eq}}, \tag{4}$$

where $\alpha_{\max}$ is determined by the equatorial pitch-angle range of a non-zero $\langle D_{\alpha\alpha}\rangle$.

Figure 7 shows the profile of ion lifetime τ^* as a function of energy [Eq. (4)]. Ions with small energies (<1 keV) are generally scattered slower than hot ions at the energy range, [1, 10] keV. The latter ion population should be isotropized and moved along the phase space density gradient toward the loss-cone within ∼10–30 min. Such hot ion losses from the magnetic hole should quickly reduce the ion pressure, and thus decrease the magnetic field depletion, i.e., ∼20 min is the timescale of magnetic hole decay. This timescale is comparable to the timescale of hole train observations by spacecraft: holes are generally observed by groups moving (or oscillating) across the spacecraft.[5,30] Although intervals of hole observations can last for hours, the spacecraft motion and hole motion do not allow spacecraft to trace

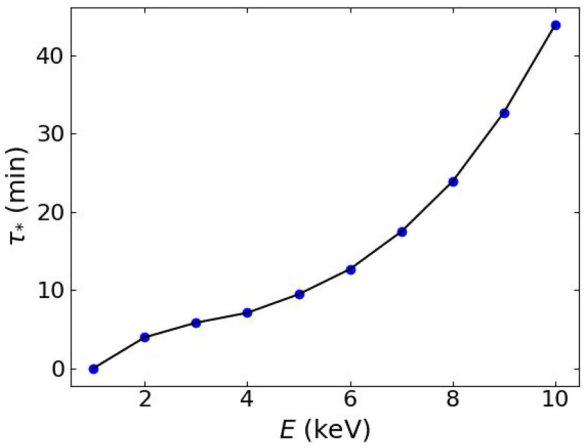

FIG. 7. Lifetime of ions scattered by EMIC waves.

dynamics of a specific hole for more than ∼10 − 30 min (see examples in Refs. 5 and 64). Therefore, the ∼20 min estimate for hole decay time does not contradict the spacecraft observations.

V. DISCUSSION AND CONCLUSIONS

In this study, we have investigated the dynamics of magnetic holes, localized magnetic depletions, which are commonly observed in the inner Earth's magnetosphere[5,12,14] and near-Earth solar wind.[55,61] These magnetic holes are pressure-balanced structures supported by the thermal pressure of a hot, transversely anisotropic ion population trapped within the hole. In the Earth's inner magnetosphere, magnetic holes are often observed as a *train* of quasiperiodic structures that further modulate electromagnetic ion cyclotron waves[5,30] and transport hot ion populations closer to the planet. In particular, large magnetic field perturbation of the most intense magnetic holes allows them to effectively scatter relativistic electrons.[56,57] All these characteristics make magnetic holes an important element for the ion kinetics of the inner magnetosphere. The formation of magnetic holes is associated with the nonlinear stage of the ion mirror instability,[8,24,31,40,47] and thus their lifetime should be controlled by the dynamics of the ion-trapped population.

The transversely anisotropic ion population inside magnetic holes can generate electromagnetic ion cyclotron waves, which may further scatter ions and reduce their contribution to the hole pressure balance. We examined two main consequences of such scattering that can result in magnetic hole decay: (1) reduction of ion anisotropy due to ion isotropization and (2) ion losses due to precipitation into the atmosphere. Even complete isotropization of the ion population cannot significantly reduce the ion contribution to the pressure balance. Thus, this mechanism does not result in magnetic hole decay, but only slightly reduces the magnetic hole's magnitude. The observed intensities of the electromagnetic ion cyclotron waves and their spectral characteristics allow these waves to effectively scatter the main (hot) ion population. The typical lifetime of this population is tens of minutes, and this estimate is quite comparable to the timescale of magnetic hole observations.[5] Therefore, this (second) mechanism is quite a prospective and the most promising candidate for magnetic hole destruction.

Based on our analysis, we propose the following probable steps for magnetic hole dynamics in the Earth's inner magnetosphere: (1) hole formation at the magnetopause due to mirror instability of hot ions that are anisotropically heated by the solar wind compression of the Earth's magnetosphere, (2) propagation (drift) of magnetic holes to the smaller radial distances due to plasma convection, (3) generation of EMIC waves within magnetic holes and hot ion scattering, and (4) precipitation of a significant fraction of hot ion population into the Earth's atmosphere and hole decay. This hypothesis assumes that the magnetic hole decay in the inner Earth's magnetosphere is contributed by two factors: the presence of cold, dense background plasma that reduces ion resonant energies and intensifies the EMIC wave generation, and the presence of loss cone (connection of magnetic field lines with the collisional atmosphere where ions can be lost). These two factors are rather unique for the inner magnetosphere conditions, and their absence in the solar wind likely explains why solar wind magnetic holes can survive for a much longer time.[42]

ACKNOWLEDGMENTS

M.F.B., A.V.A., and X.-J. Z. acknowledge support from NASA (Grant Nos. 80NSSC20K1270 and 80NSSC23K0403). X.-J. Z. acknowledges support from NASA (Grant No. 80NSSC20K0689) and NSF (Grant No. 2329897). We also acknowledge support from NASA (No. NAS5-02099).

AUTHOR DECLARATIONS

Conflict of Interest

The authors have no conflicts to disclose.

Author Contributions

Muhammad Shahid: Data curation (equal); Formal analysis (equal); Investigation (equal); Software (equal); Visualization (equal); Writing – original draft (equal). **M. Fraz Bashir:** Conceptualization (equal); Funding acquisition (equal); Investigation (equal); Methodology (equal); Software (equal); Supervision (equal); Validation (equal); Visualization (equal); Writing – review & editing (equal). **Anton V. Artemyev:** Conceptualization (equal); Funding acquisition (equal); Investigation (equal); Methodology (equal); Software (equal); Supervision (equal); Validation (equal); Visualization (equal); Writing – review & editing (equal). **Xiao-Jia Zhang:** Conceptualization (equal); Funding acquisition (equal); Investigation (equal); Validation (equal); Writing – review & editing (equal). **Vassilis Angelopoulos:** Funding acquisition (equal); Resources (equal); Supervision (equal); Validation (equal); Writing – review & editing (equal). **G. Murtaza:** Supervision (equal); Validation (equal); Writing – review & editing (equal).

DATA AVAILABILITY

The data that support the findings of this study are openly available in THEMIS at http://doi.org/10.1007/s11214-018-0576-4, Ref. 3.

REFERENCES

[1]J. M. Albert and Y. Y. Shprits, "Estimates of lifetimes against pitch angle diffusion," J. Atmos. Sol. Terrestrial Phys. **71**, 1647–1652 (2009).
[2]V. Angelopoulos, "The THEMIS mission," Space Sci. Rev **141**, 5–34 (2008).
[3]V. Angelopoulos, P. Cruce, A. Drozdov, E. W. Grimes, N. Hatzigeorgiu, D. A. King, D. Larson, J. W. Lewis, J. M. McTiernan, D. A. Roberts, C. L. Russell, T. Hori, Y. Kasahara, A. Kumamoto, A. Matsuoka, Y. Miyashita, Y. Miyoshi, I. Shinohara, M. Teramoto, J. B. Faden, A. J. Halford, M. McCarthy, R. M. Millan, J. G. Sample, D. M. Smith, L. A. Woodger, A. Masson, A. A. Narock, K. Asamura, T. F. Chang, C. Y. Chiang, Y. Kazama, K. Keika, S. Matsuda, T. Segawa, K. Seki, M. Shoji, S. W. Y. Tam, N. Umemura, B. J. Wang, S. Y. Wang, R. Redmon, J. V. Rodriguez, H. J. Singer, J. Vandegriff, S. Abe, M. Nose, A. Shinbori, Y. M. Tanaka, S. UeNo, L. Andersson, P. Dunn, C. Fowler, J. S. Halekas, T. Hara, Y. Harada, C. O. Lee, R. Lillis, D. L. Mitchell, M. R. Argall, K. Bromund, J. L. Burch, I. J. Cohen, M. Galloy, B. Giles, A. N. Jaynes, O. Le Contel, M. Oka, T. D. Phan, B. M. Walsh, J. Westlake, F. D. Wilder, S. D. Bale, R. Livi, M. Pulupa, P. Whittlesey, A. DeWolfe, B. Harter, E. Lucas, U. Auster, J. W. Bonnell, C. M. Cully, E. Donovan, R. E. Ergun, H. U. Frey, B. Jackel, A. Keiling, H. Korth, J. P. McFadden, Y. Nishimura, F. Plaschke, P. Robert, D. L. Turner, J. M. Weygand, R. M. Candey, R. C. Johnson, T. Kovalick, M. H. Liu, R. E. McGuire, A. Breneman, K. Kersten, and P. Schroeder, "The Space Physics Environment Data Analysis System (SPEDAS) space," Sci. Rev **215**, 9 (2019).
[4]H. U. Auster, K. H. Glassmeier, W. Magnes, O. Aydogar, W. Baumjohann, D. Constantinescu, D. Fischer, K. H. Fornacon, E. Georgescu, P. Harvey, O. Hillenmaier, R. Kroth, M. Ludlam, Y. Narita, R. Nakamura, K. Okrafka, F. Plaschke, I. Richter, H. Schwarzl, B. Stoll, A. Valavanoglou, and M. Wiedemann, "The THEMIS fluxgate magnetometer," Space Sci. Rev **141**, 235–264 (2008).
[5]M. F. Bashir, A. Artemyev, X. J. Zhang, and V. Angelopoulos, "Energetic electron precipitation driven by the combined effect of ULF, EMIC, and whistler waves," J. Geophys. Res. (Space Phys.) **127**, e29871 (2022).
[6]M. F. Bashir, A. Artemyev, X. J. Zhang, and V. Angelopoulos, "Hot plasma effects on electron resonant scattering by electromagnetic ion cyclotron waves," Geophys. Res. Lett. **49**, e99229 (2022).
[7]L. W. Blum, A. Halford, R. Millan, J. W. Bonnell, J. Goldstein, M. Usanova, M. Engebretson, M. Ohnsted, G. Reeves, H. Singer, M. Clilverd, and X. Li, "Observations of coincident EMIC wave activity and duskside energetic electron precipitation on 18–19 January 2013," Geophys. Res. Lett. **42**, 5727–5735, https://doi.org/10.1002/2015GL065245 (2015).
[8]F. Califano, P. Hellinger, E. Kuznetsov, T. Passot, P. L. Sulem, and P. M. TráVníčEk, "Nonlinear mirror mode dynamics: Simulations and modeling," J. Geophys. Res. **113**, A08219 (2008).
[9]X. Cao, B. Ni, J. Liang, Z. Xiang, Q. Wang, R. Shi, X. Gu, C. Zhou, Z. Zhao, S. Fu, and J. Liu, "Resonant scattering of central plasma sheet protons by multiband EMIC waves and resultant proton loss timescales," J. Geophys. Res. (Space Phys.) **121**, 1219–1232, https://doi.org/10.1002/2015JA021933 (2016).
[10]X. Cao, B. Ni, D. Summers, Y. Y. Shprits, X. Gu, S. Fu, Y. Lou, Y. Zhang, X. Ma, W. Zhang, H. Huang, and J. Yi, "Sensitivity of EMIC wave-driven scattering loss of ring current protons to wave normal angle distribution," Geophys. Res. Lett. **46**, 590–598, https://doi.org/10.1029/2018GL081550 (2019).
[11]L. Chen, R. M. Thorne, and J. Bortnik, "The controlling effect of ion temperature on EMIC wave excitation and scattering," Geophys. Res. Lett. **38**, L16109 (2011).
[12]R. Chen, X. Gao, Q. Lu, B. T. Tsurutani, H. Chen, and S. Wang, "First observation of electron cyclotron harmonic waves inside mirror mode structures in the earth's outer magnetosphere," Geophys. Res. Lett. **49**, e97592 (2022).
[13]R. Chen, X. Gao, Q. Lu, B. T. Tsurutani, Y. Miyoshi, X. Zhou, Y. Ke, H. Chen, and J. Ma, "Observation of whistler mode waves inside mirror mode structures in the earth's outer magnetosphere," J. Geophys. Res. (Space Phys.) **128**, e2023JA031792, https://doi.org/10.1029/2023JA031792 (2023).
[14]M. B. Cooper, A. J. Gerrard, L. J. Lanzerotti, A. R. Soto-Chavez, H. Kim, I. V. Kuzichev, and L. V. Goodwin, "Mirror instabilities in the inner magnetosphere and their potential for localized ULF wave generation," J. Geophys. Res. (Space Phys.) **126**, e28773 (2021).
[15]J. M. Cornwall, F. V. Coroniti, and R. M. Thorne, "Turbulent loss of ring current protons," J. Geophys. Res. **75**, 4699, https://doi.org/10.1029/JA075i025p04699 (1970).
[16]X. Duanmu, Z. Yao, Y. Wei, and S. Ye, "Two types of mirror mode waves in the Kronian magnetosheath," Earth Planet. Phys. **7**, 414–420 (2023).
[17]Y. Ebihara, M. C. Fok, J. B. Blake, and J. F. Fennell, "Magnetic coupling of the ring current and the radiation belt," J. Geophys. Res. **113**, 7221 (2008).

[18]V. Génot, P. Louarn, and F. Mottez, "Fast evolving spatial structure of auroral parallel electric fields," J. Geophys. Res. **106**, 29633–29644, https://doi.org/10.1029/2001JA000076 (2001).
[19]K. H. Glassmeier, U. Motschmann, C. Mazelle, F. M. Neubauer, K. Sauer, S. A. Fuselier, and M. H. Acuna, "Mirror modes and fast magnetoacoustic waves near the magnetic pileup boundary of comet P/Halley," J. Geophys. Res. **98**, 20955–20964, https://doi.org/10.1029/93JA02582 (1993).
[20]S. A. Glauert and R. B. Horne, "Calculation of pitch angle and energy diffusion coefficients with the PADIE code," J. Geophys. Res. **110**, 4206 (2005).
[21]C. T. Haynes, D. Burgess, E. Camporeale, and T. Sundberg, "Electron vortex magnetic holes: A nonlinear coherent plasma structure," Phys. Plasmas **22**, 012309 (2015).
[22]P. Hellinger, "Comment on the linear mirror instability near the threshold," Phys. Plasmas **14**, 082105 (2007).
[23]P. Hellinger, P. Trávníček, J. C. Kasper, and A. J. Lazarus, "Solar wind proton temperature anisotropy: Linear theory and WIND/SWE observations," Geophys. Res. Lett. **33**, 9101 (2006).
[24]P. Hellinger and P. M. Trávníček, "Proton temperature-anisotropy-driven instabilities in weakly collisional plasmas: Hybrid simulations," J. Plasma Phys. **81**, 305810103 (2015).
[25]S. Y. Huang, J. W. Du, F. Sahraoui, Z. G. Yuan, J. S. He, J. S. Zhao, O. Le Contel, H. Breuillard, D. D. Wang, X. D. Yu, X. H. Deng, H. S. Fu, M. Zhou, C. J. Pollock, R. B. Torbert, C. T. Russell, and J. L. Burch, "A statistical study of kinetic-size magnetic holes in turbulent magnetosheath: MMS observations," J. Geophys. Res. (Space Phys.) **122**, 8577–8588, https://doi.org/10.1002/2017JA024415 (2017).
[26]X. F. Ji, X. G. Wang, W. J. Sun, C. J. Xiao, Q. Q. Shi, J. Liu, and Z. Y. Pu, "EMHD theory and observations of electron solitary waves in magnetotail plasmas," J. Geophys. Res. **119**, 4281–4289, https://doi.org/10.1002/2014JA019924 (2014).
[27]T. Karlsson, H. Trollvik, S. Raptis, H. Nilsson, and H. Madanian, "Solar wind magnetic holes can cross the bow shock and enter the magnetosheath," Ann. Geophys. **40**, 687–699 (2022).
[28]C. F. Kennel, "Consequences of a magnetospheric plasma," Rev. Geophys. (Space Phys.) **7**, 379–419 (1969).
[29]H. Kim, K. Shiokawa, J. Park, Y. Miyoshi, Y. Miyashita, C. Stolle, H. K. Connor, J. Hwang, S. Buchert, H. J. Kwon, S. Nakamura, K. Nakamura, S. I. Oyama, Y. Otsuka, T. Nagatsuma, and K. Sakaguchi, "Isolated proton aurora driven by EMIC Pc1 wave: PWING, swarm, and NOAA POES multi-instrument observations," Geophys. Res. Lett. **48**, e95090 (2021).
[30]N. Kitamura, M. Shoji, S. Nakamura, M. Kitahara, T. Amano, Y. Omura, H. Hasegawa, S. A. Boardsen, Y. Miyoshi, Y. Katoh, M. Teramoto, Y. Saito, S. Yokota, M. Hirahara, D. J. Gershman, B. L. Giles, C. T. Russell, R. J. Strangeway, N. Ahmadi, P. A. Lindqvist, R. E. Ergun, S. A. Fuselier, and J. L. Burch, "Energy transfer between hot protons and electromagnetic ion cyclotron waves in compressional Pc5 ultra low frequency waves," J. Geophys. Res. (Space Phys.) **126**, e28912 (2021).
[31]E. A. Kuznetsov, T. Passot, and P. L. Sulem, "Dynamical model for nonlinear mirror modes near threshold," Phys. Rev. Lett. **98**, 235003 (2007).
[32]Z. Y. Li, W. J. Sun, X. G. Wang, Q. Q. Shi, C. J. Xiao, Z. Y. Pu, X. F. Ji, S. T. Yao, and S. Y. Fu, "An EMHD soliton model for small-scale magnetic holes in magnetospheric plasmas," J. Geophys. Res. **121**, 4180–4190, https://doi.org/10.1002/2016JA022424 (2016).
[33]J. Liang, D. Gillies, E. Donovan, H. Parry, I. Mann, M. Connors, and E. Spanswick, "On the green isolated proton auroras during Canada thanksgiving geomagnetic storm," Front. Astron. Space Sci. **9**, 1040092 (2022).
[34]L. R. Lyons, "Pitch angle and energy diffusion coefficients from resonant interactions with ion-cyclotron and whistler waves," J. Plasma Phys. **12**, 417–432 (1974).
[35]J. P. McFadden, C. W. Carlson, D. Larson, M. Ludlam, R. Abiad, B. Elliott, P. Turin, M. Marckwordt, and V. Angelopoulos, "The THEMIS ESA plasma instrument and in-flight calibration," Space Sci. Rev **141**, 277–302 (2008).
[36]K. Nakamura, K. Shiokawa, M. Nosé, T. Nagatsuma, K. Sakaguchi, H. Spence, G. Reeves, H. O. Funsten, R. MacDowall, C. Smith, J. Wygant, J. Bonnell, and I. R. Mann, "Multi-event study of simultaneous observations of isolated proton auroras at subauroral latitudes using ground all-sky imagers and the Van Allen probes," J. Geophys. Res. (Space Phys.) **127**, e30455 (2022).
[37]S. J. Noh, D. Y. Lee, H. Kim, L. J. Lanzerotti, A. Gerrard, and R. M. Skoug, "Upper limit of proton anisotropy and its relation to electromagnetic ion cyclotron waves in the inner magnetosphere," J. Geophys. Res. (Space Phys.) **126**, e28614 (2021).
[38]K. G. Orlova and Y. Y. Shprits, "On the bounce-averaging of scattering rates and the calculation of bounce period," Phys. Plasmas **18**, 092904 (2011).
[39]O. A. Pokhotelov, R. A. Treumann, R. Z. Sagdeev, M. A. Balikhin, O. G. Onishchenko, V. P. Pavlenko, and I. Sandberg, "Linear theory of the mirror instability in non-Maxwellian space plasmas," J. Geophys. Res. (Space Phys.) **107**, 1312 (2002).
[40]P. Porazik and J. R. Johnson, "Gyrokinetic particle simulation of nonlinear evolution of mirror instability," J. Geophys. Res. (Space Phys.) **118**, 7211–7218, https://doi.org/10.1002/2013JA019308 (2013).
[41]V. Roytershteyn, H. Karimabadi, and A. Roberts, "Generation of magnetic holes in fully kinetic simulations of collisionless turbulence," Philos. Trans. R. Soc. A **373**, 20140151 (2015).
[42]C. T. Russell, L. K. Jian, J. G. Luhmann, T. L. Zhang, F. M. Neubauer, R. M. Skoug, X. Blanco-Cano, N. Omidi, and M. M. Cowee, "Mirror mode waves: Messengers from the coronal heating region," Geophys. Res. Lett. **35**, L15101 (2008).
[43]C. T. Russell, W. Riedler, K. Schwingenschuh, and Y. Yeroshenko, "Mirror instability in the magnetosphere of comet Halley," Geophys. Res. Lett. **14**, 644–647, https://doi.org/10.1029/GL014i006p00644 (1987).
[44]D. Schmid, M. Volwerk, F. Plaschke, Z. Vörös, T. L. Zhang, W. Baumjohann, and Y. Narita, "Mirror mode structures near Venus and Comet P/Halley," Ann. Geophys. **32**, 651–657 (2014).
[45]P. I. Shustov, A. V. Artemyev, A. S. Volokitin, I. Y. Vasko, X. J. Zhang, and A. A. Petrukovich, "Electron magnetosonic waves and sub-ion magnetic holes in the magnetotail plasma," Phys. Plasmas **29**, 012902 (2022).
[46]C. Simon Wedlund, M. Volwerk, C. Mazelle, J. Halekas, D. Rojas-Castillo, J. Espley, and C. Möstl, "Making waves: mirror mode structures around mars observed by the MAVEN spacecraft," J. Geophys. Res. (Space Phys.) **127**, e29811 (2022).
[47]A. R. Soto-Chavez, L. J. Lanzerotti, J. W. Manweiler, A. Gerrard, R. Cohen, Z. Xia, L. Chen, and H. Kim, "Observational evidence of the drift-mirror plasma instability in Earth's inner magnetosphere," Phys. Plasmas **26**, 042110 (2019).
[48]D. J. Southwood and M. G. Kivelson, "Mirror instability. I—Physical mechanism of linear instability," J. Geophys. Res. **98**, 9181–9187, https://doi.org/10.1029/92JA02837 (1993).
[49]T. H. Stix, *The Theory of Plasma Waves* (McGraw-Hill Book Co., 1962).
[50]D. Summers and R. M. Thorne, "Relativistic electron pitch-angle scattering by electromagnetic ion cyclotron waves during geomagnetic storms," J. Geophys. Res. **108**, 1143 (2003).
[51]A. Tello Fallau, C. Goetz, C. S. Wedlund, M. Volwerk, and A. Moeslinger, "Revisiting mirror modes in the plasma environment of comet 67P/Churyumov-Gerasimenko," Ann. Geophys. **41**, 569–587 (2023).
[52]M. E. Usanova, A. Drozdov, K. Orlova, I. R. Mann, Y. Shprits, M. T. Robertson, D. L. Turner, D. K. Milling, A. Kale, D. N. Baker, S. A. Thaller, G. D. Reeves, H. E. Spence, C. Kletzing, and J. Wygant, "Effect of EMIC waves on relativistic and ultrarelativistic electron populations: Ground-based and Van Allen Probes observations," Geophys. Res. Lett. **41**, 1375–1381, https://doi.org/10.1002/2013GL059024 (2014).
[53]M. E. Usanova, I. R. Mann, J. Bortnik, L. Shao, and V. Angelopoulos, "THEMIS observations of electromagnetic ion cyclotron wave occurrence: Dependence on AE, SYMH, and solar wind dynamic pressure," J. Geophys. Res. **117**, 10218 (2012).
[54]M. Volwerk, C. S. Wedlund, D. Mautner, S. Rojas Mata, G. Stenberg Wieser, Y. Futaana, C. Mazelle, D. Rojas-Castillo, C. Bertucci, and M. Delva, "Statistical distribution of mirror-mode-like structures in the magnetosheaths of unmagnetized planets—Part 2: Venus as observed by the Venus Express spacecraft," Ann. Geophys. **41**, 389–408 (2023).
[55]G. Q. Wang, M. Volwerk, S. D. Xiao, M. Y. Wu, Y. Q. Chen, and T. L. Zhang, "Foreshock as a source region of electron-scale magnetic holes in the solar wind at 1 AU," Astrophys. J. **915**, 3 (2021).
[56]Y. Xiong, L. Chen, L. Xie, S. Fu, Z. Xia, and Z. Pu, "Relativistic electron's butterfly pitch angle distribution modulated by localized background magnetic

field perturbation driven by hot ring current ions," Geophys. Res. Lett. **44**, 4393–4400, https://doi.org/10.1002/2017GL072558 (2017).
[57]Y. Xiong, L. Xie, S. Fu, and Z. Pu, "Statistical study of energetic electron butterfly pitch angle distributions during magnetic dip events," Geophys. Res. Lett. **46**, 13,621–13,629, https://doi.org/10.1029/2019GL085091 (2019).
[58]S. T. Yao, M. Hamrin, Q. Q. Shi, Z. H. Yao, A. W. Degeling, Q. G. Zong, H. Liu, A. M. Tian, J. Liu, H. Q. Hu, B. Li, S. C. Bai, C. T. Russell, and B. L. Giles, "Propagating and dynamic properties of magnetic dips in the dayside magnetosheath: MMS observations," J. Geophys. Res. (Space Phys.) **125**, e26736 (2020).
[59]Z. F. Yin, X. Z. Zhou, Z. J. Hu, C. Yue, Q. G. Zong, Y. X. Hao, Z. Y. Liu, X. R. Chen, L. Li, S. Y. Fu, H. O. Funsten, and J. W. Manweiler, "Localized excitation of electromagnetic ion cyclotron waves from anisotropic protons filtered by magnetic dips," J. Geophys. Res. (Space Phys.) **127**, e30531 (2022).
[60]Z. F. Yin, X. Z. Zhou, Q. G. Zong, Z. Y. Liu, C. Yue, Y. Xiong, L. Xie, Y. F. Wang, and S. Y. Fu, "Inner magnetospheric magnetic dips and energetic protons trapped therein: Multi spacecraft observations and simulations," Geophys. Res. Lett. **48**, e92567 (2021).
[61]L. Yu, S. Y. Huang, Z. G. Yuan, K. Jiang, Y. Y. Wei, J. Zhang, S. B. Xu, Q. Y. Xiong, Z. Wang, R. T. Lin, Y. J. Li, C. M. Wang, and G. J. Song, "Small-scale magnetic holes in the solar wind observed by Parker Solar probe," J. Geophys. Res. (Space Phys.) **127**, e30505 (2022).
[62]C. Yue, J. Bortnik, R. M. Thorne, Q. Ma, X. An, C. R. Chappell, A. J. Gerrard, L. J. Lanzerotti, Q. Shi, G. D. Reeves, H. E. Spence, D. G. Mitchell, M. Gkioulidou, and C. A. Kletzing, "The characteristic pitch angle distributions of 1 eV to 600 keV protons near the equator based on Van Allen probes observations," J. Geophys. Res. **12**, 9464–9473 (2017).
[63]C. Yue, C. W. Jun, J. Bortnik, X. An, Q. Ma, G. D. Reeves, H. E. Spence, A. J. Gerrard, M. Gkioulidou, D. G. Mitchell, and C. A. Kletzing, "The relationship between EMIC wave properties and proton distributions based on Van Allen probes observations," Geophys. Res. Lett. **46**, 4070–4078, https://doi.org/10.1029/2019GL082633 (2019).
[64]X. J. Zhang, L. Chen, A. V. Artemyev, V. Angelopoulos, and X. Liu, "Periodic excitation of chorus and ECH waves modulated by ultralow frequency compressions," J. Geophys. Res. (Space Phys.) **124**, 8535–8550, https://doi.org/10.1029/2019JA027201 (2019).
[65]Y. Zhao, H. Zhu, and H. Chen, "Expected EMIC wave generation and unexpected MS wave disruption in a magnetic dip," J. Geophys. Res. (Space Phys.) **128**, e2023JA031776, https://doi.org/10.1029/2023JA031776 (2023).
[66]H. Zhu, L. Chen, A. V. Artemyev, X. J. Zhang, and A. W. Breneman, "Superposed epoch analyses of electron-driven and proton-driven magnetic dips," Geophys. Res. Lett. **48**, e94934 (2021).
[67]H. Zhu, L. Chen, S. G. Claudepierre, and L. Zheng, "Direct evidence of the pitch angle scattering of relativistic electrons induced by EMIC waves," Geophys. Res. Lett. **47**, e2019GL085637, https://doi.org/10.1029/2019GL085637 (2020).
[68]H. Zhu, L. Chen, and Z. Xia, "Electron-driven magnetic dip embedded within the proton-driven magnetic dip and the related echoes of butterfly distribution of relativistic electrons," Geophys. Res. Lett. **47**, e88983 (2020).